Neuron, Vol. 18, 153–166, January, 1997, Copyright ©1997 by Cell Press

Identification of Functionally Distinct Isoforms of the N-Type Ca^{2+} Channel in Rat Sympathetic Ganglia and Brain

Zhixin Lin, Stephanie Haus, Jeremy Edgerton, and Diane Lipscombe
Department of Neuroscience
Brown University
Providence, RI 02912

Summary

The N channel is critical for regulating release of neurotransmitter at many synapses, and even subtle differences in its activity would be expected to influence the efficacy of synaptic transmission. Although several splice variants of the N channel are expressed in the mammalian nervous system, their biological importance is presently unclear. Here, we show that variants of the α_{1B} subunit of the N channel are expressed in sympathetic ganglia and that alternative splicing within IIIS3-S4 and IVS3-S4 generate kinetically distinct channels. We further show a striking difference between the expression pattern of the S3-S4 variants in brain and peripheral ganglia and conclude that the brain-dominant form of the N channel gates 2- to 4-fold more rapidly than that predominant in ganglia.

Introduction

The major pharmacological and functional determinants of the N-type Ca^{2+} channel are contained in the α_{1B} subunit (Dubel et al., 1992; Williams et al., 1992; Fujita et al., 1993; Stea et al., 1993; Ellinor et al., 1994) while the Ca^{2+} channel β-subunit family is thought to be critical for enabling reconstitution of N channels with normal gating kinetics (Williams et al., 1992; Fujita et al., 1993; Stea et al., 1993) and for mediating modulatory effects of second messengers (Roche et al., 1995; Stea et al., 1995; Dolphin 1996). To date, several different clones of α_{1B}, sharing >90% overall homology, have been isolated from rat and rabbit brain and from human and mouse neuroblastoma cell lines, which are distinguishable on the basis of short, highly localized regions of sequence divergence (Williams et al., 1992; Coppola et al., 1994). There is some suggestion that variants of α_{1B} encode functionally different N channels (Dubel et al., 1994, Soc. Neurosci., abstract), but a detailed analysis of the potential significance of these variants is currently lacking. Given the central role that the N channel plays in regulating the release of transmitter from sympathetic neurons (Hirning et al., 1988) and certain central synapses (Luebke et al., 1993; Takahashi and Momiyama, 1993; Wheeler et al., 1994; Dunlap et al., 1995), it is possible that the expression of different splice variants of the N channel might provide a mechanism for fine-tuning transmission efficacy at different synapses.

A series of detailed kinetic analyses of macroscopic and single N channel currents in peripheral neurons has indeed suggested that kinetically distinct forms of the N channel are expressed in the nervous system, distinguished by different channel open probabilities (Bean, 1989a; Lipscombe et al., 1989; Delcour et al., 1993; Rittenhouse and Hess, 1994), single channel conductances (Plummer et al., 1989), and rates of inactivation (Jones and Marks, 1989; Kongsamut et al., 1989; Plummer et al., 1989; Plummer and Hess, 1991; Cox and Dunlap, 1994). Almost exclusively, however, conformational changes within individual N channel molecules are invoked to account for the presence of kinetically distinct N channel currents in recordings from native cells. Of the kinetic models that have been proposed to account for the apparent complex gating behavior of the N channel, most incorporate two to three distinct channel open states or gating modes (Bean, 1989a; Elmslie et al., 1990; Delcour et al., 1993; Rittenhouse and Hess, 1994). The existence of kinetically distinct, but as yet molecularly undefined N channels is elevated from the status of biophysical curiosity to the functionally relevant by the now generally accepted theory that these different gating behaviors may provide the basis for understanding the mechanism of G protein–mediated modulation of the N channel (Bean, 1989a; Hille, 1992a). Surprisingly, relatively little attention has been paid to the possibility that the presence of kinetically distinct N channel currents might arise from the expression of structurally and functionally different channel isoforms.

Ultimately a detailed picture of the important elements regulating the gating of the N channel will depend critically on a direct correlation between molecular structure and channel behavior. With this in mind and in view of the fact that most molecular and biochemical analyses of the N channel to date have relied on brain and related neuronal cell lines, we set out to determine the precise composition of the major molecular components underlying the N channel expressed in a functionally and electrophysiologically well characterized group of peripheral neurons. As a result, we were able to identify and characterize the most abundantly expressed variants of the Ca^{2+} channel α_{1B} subunit expressed in rat sympathetic ganglia and subsequently to demonstrate an unexpected reciprocal pattern of expression of N channel variants in brain compared to sympathetic ganglia.

Results

Multiple Variants of α_{1B} Are Expressed in Rat Sympathetic Ganglia

Fifty-seven clones containing α_{1B} sequence were isolated by hybridization screening of an oligo dT–primed rat superior cervical ganglia (SCG) cDNA library (inserts of 4–5 kb; see Experimental procedures) using a NotI–SpeI fragment of full length rbB-1 (nt 25–8768; Dubel et al., 1992). Polymerase chain reaction (PCR) and restriction digest analysis of five of these clones indicated the presence of at least two variants of rat SCG-derived α_{1B} cDNAs in the library. Figure 1A shows that α_{1B} cDNA clones, rscg9407 and rscg9408, differ in length by ~2.5 kb in the region between nt5015 (located near the 3′ end of the coding region) and the bracketing T7 promoter in the vector. After completely sequencing the 3′UTR of

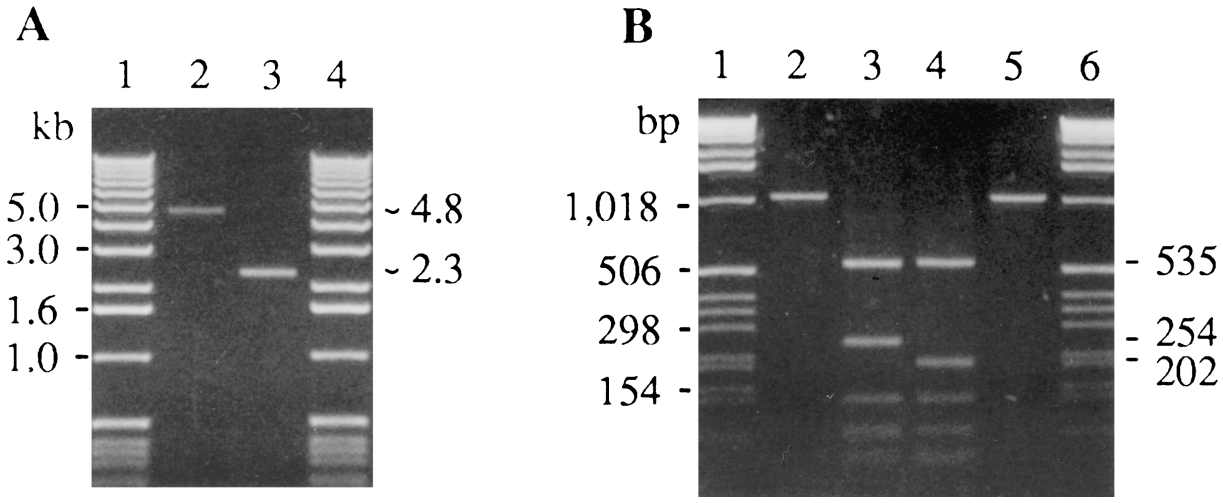

Figure 1. Identification of Variants of the N-Channel α_{1B} Subunit in Rat Sympathetic Ganglia

(A) PCR-derived cDNA products (nt5015 to bracketing T7 promotor) amplified from two rat sympathetic ganglia cDNA clones; rscg9407 (lane 2) and rscg9408 (lane 3). Single bands, at ~4.8 kb for rscg9407 and 2.3 kb for rscg9408, are shown separated in a 0.8% agarose gel. Double-stranded cDNA markers are shown in lanes 1 and 4. To facilitate amplification of long fragments, Taq Extender (Stratagene) was added to the PCR mix. (B) PCR-derived cDNA products (nt3460–nt4479) amplified from the rat brain-derived clone rbB-I (lanes 2 and 3) and rscg9408 (lanes 5 and 4), before (lanes 2 and 5) and after (lanes 3 and 4) digestion with DdeI. PCR amplification of both clones yields a cDNA product close to 1018 bp (lanes 2 and 5). Subsequent DdeI digest of the respective PCR-derived cDNAs reveals sequence divergence between rbB-I (lane 3) and rscg9408 (lane 4). The predicted DdeI restriction pattern in this region (nt3460–nt4479) for rbB-I is 535, 254, 134, 78, and 40 bp (lane 3). The absence of the four amino acids SFMG in rscg9408 introduces a DdeI restriction site to yield products 535, 202, 134, 78, 40, and 39 bp (lane 4).

clone rscg9408, we found it contained only 194 bases upstream of the poly(A) tail. The 3′UTR of clone rscg9407, on the other hand, contained at least 2.6 kb of 3′UTR, the first 194 bases of which were identical to the 3′UTR of clone rscg9408. Further analysis led to three observations that suggest that the truncated 3′UTR identified in clone rscg9408 is an authentic variant of the α_{1B} transcript and not a cloning artifact. We have confirmed the presence of: (1) at least 33 adenosine bases at the 3′ tail of clone rscg9408; (2) the predicted AAUAAA polyadenylation recognition site at nt7184–7189, 16 nt upstream of the poly (A) tail of clone rscg9408 and; (3) four additional clones with 194 base 3′UTRs from a PCR screen of all 57 rat SCG-derived α_{1B} clones. We also partially sequenced the long 3′ UTR contained in rscg9407, and confirmed: (1) the presence of a poly(A) tail and; (2) sequence identity to the 3′UTR of the rat brain–derived clone, rbB-I (Dubel et al., 1992). Consistent with the relatively low abundance (~10%) of α_{1B} clones with truncated 3′UTRs isolated from our sympathetic ganglia cDNA library, we can only detect a single band at 9.5–10 kb in Northern blots probed with rbB-I corresponding to α_{1B} mRNA with full-length 3′UTRs (Z. L. and D. L., unpublished data).

We completely sequenced three overlapping clones that represented the entire length of the coding region of the α_{1B} gene and systematically analyzed five more α_{1B} cDNA clones derived from our rat SCG cDNA libraries. As a result, we identified four discrete sites where the sequence differed from the rat brain–derived clone, rbB-I. Namely, (1) a single base change (A→G at nt530) resulting in an amino acid change, Glu177→Gly177 in the putative transmembrane region, IS3; (2) a three-base deletion (Δnt1243–1245), which removes the amino acid Ala415 from the putative intracellular loop between IS6-IIS1 in α_{1B}; (3) a 12-base deletion (Δnt3705–3716) encoding a tetrapeptide sequence, Ser-Phe-Met-Gly (SFMG; Figure 1B) residing in the putative extracellular loop between IIIS3-IIIS4 in rbB-I and; (4) a six-base insertion (between nt4674–5) creating a two amino acid insertion, Glu–Thr (ET), in the putative extracellular loop between IVS3–IVS4 of α_{1B}. An example of the analysis used to identify these variants is shown in Figure 1B, which compares a DdeI-restriction digest of PCR-derived cDNAs amplified from clone rscg9408 with that from the rat brain–derived clone rbB-I (Dubel et al., 1992). The DdeI digest can distinguish between clones differing in the expression of the SFMG site at nt3705–3716. Apart from the four sites listed above, the DNA sequence of the three overlapping clones was identical to rbB-I. Three of the four variant sites within the coding region of α_{1B}, identified in the present study in rat sympathetic neurons (i.e., G177, ΔA415, and ΔSFMG) have also been identified in an α_{1B} clone derived from rat brain (rbB-II) (see Figure 7) (Dubel et al., 1994, Soc. Neurosci., abstract; Stea et al., 1995). In addition, sequence comparisons between α_{1B} clones isolated from several other mammalian neuronal preparations are consistent with A415 and ET being potential sites of RNA splicing (see Figure 7).

Partial Linkage Analysis of the Potential Splice Sites in α_{1B} Expressed in Sympathetic Ganglia

We were next interested to determine how many additional variants of α_{1B} might be expressed in sympathetic ganglia. cDNA clones containing multiple variant sites cannot be readily isolated, however, primarily because of the wide dispersion of these sites (G177 and the ET

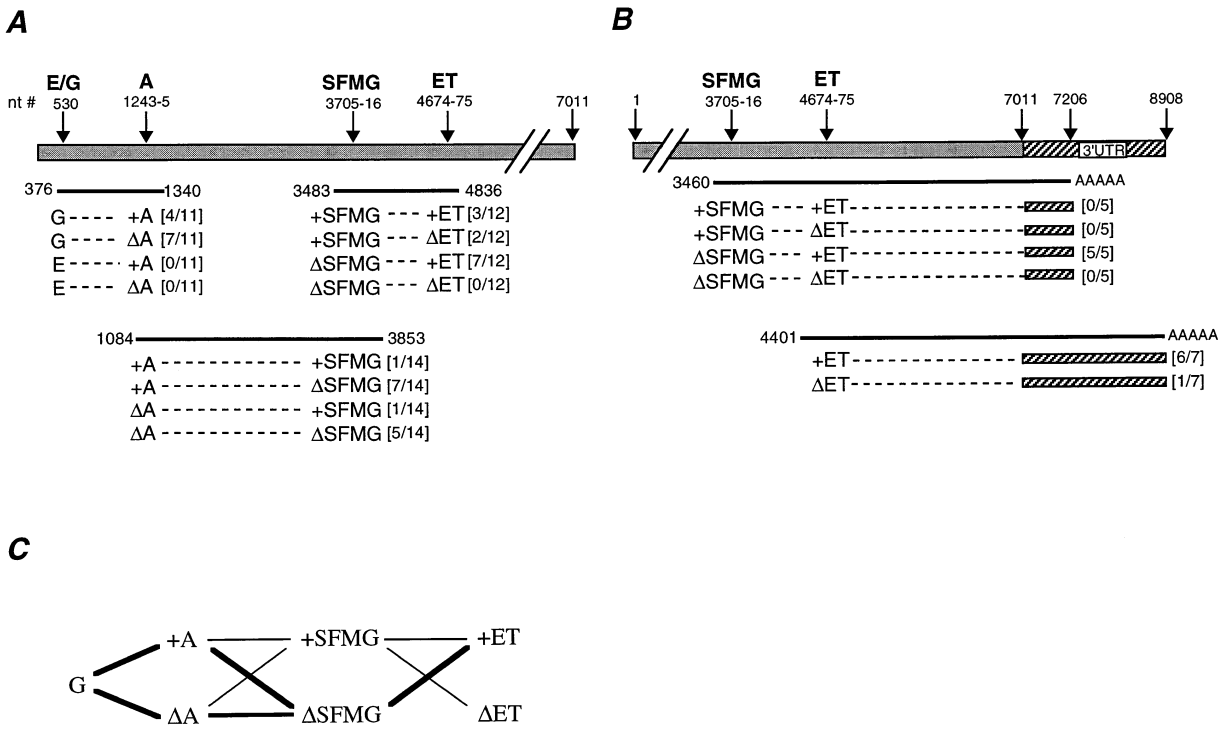

Figure 2. Analysis of Five Potential Sites of Sequence Variation in Ca^{2+} Channel α_{1B} Transcripts Present in Rat Sympathetic Ganglia

(A) Summary of the analysis of PCR-derived cDNAs obtained from RT-PCR amplification of rat sympathetic ganglia mRNA using three sets of primers. PCR-derived products (nt376→nt1340, nt1084→nt3853, and nt3483→nt4836) were subcloned and analyzed at four sites (E/G, A, SFMG, and ET) whose amino acid sequence, relative position, and nucleotide location are indicated (arrows) on a map of rbB-I (nt1–7011; top). A total of 37 PCR-derived clones were analyzed, and the frequencies of occurrence of each pair of variant sites, within each of the three groups, are indicated in brackets.

(B) Analysis of 12 of the longest α_{1B} cDNAs (up to 5.4 kb) derived from a poly T–primed rat sympathetic ganglia cDNA library. Top, the relative position of SFMG and ET and the truncation site within the 3′UTR are indicated on a map of rbB-I (arrows). The relative positions of the coding region and of the 3′UTR of α_{1B} are represented by the solid shading and diagonal fill, respectively. Middle, restriction analysis of five α_{1B} clones containing truncated 3′UTRs, and which extend to at least nt3460, indicate that all five clones lack SFMG but contain ET (brackets). Bottom, restriction analysis of seven α_{1B} clones containing the full-length 3′UTR, and which extend to at least nt4501, indicates that ET-containing clones dominate (brackets).

(C) Predicted composition of variants of α_{1B} mRNA expressed in rat sympathetic ganglia, based on the analysis summarized in A and B. Up to six different variants of α_{1B} mRNA could be expressed in sympathetic ganglia. The heavy lines indicate the most abundantly observed sequences (ΔSFMG, +ET); thin lines indicate the less frequently observed sequences (+SFMG, ΔET). A415 containing and A415 lacking sequences were equally abundant, and G177 was invariant.

site are >4.1 kb apart; Figures 2A and 2B). Therefore, to further characterize the variant sites in α_{1B}, to determine their relative abundance in the ganglia and their potential association with each other within the same transcript, we devised a PCR-based approach for a "nearest neighbor" linkage analysis. In this approach, we designed three sets of primers for the reverse transcriptase (RT)-PCR amplification of cDNA regions, each containing one of the three pairs of nearest neighbor sites (i.e., E/G177 → ±A415; ±A415 → ±SFMG and; ±SFMG → ±ET). Within a given reaction, the PCR primers would be expected to amplify variant transcripts equally well. We then subcloned and analyzed, by restriction digest and DNA sequencing, the pool of PCR-derived cDNA products from each group (Figure 2A). The relative abundance of each variant site among the subclones thus provided us with an estimate of the relative abundance of these sequences in the SCG mRNA pool. The following questions were addressed: (1) how many different variants of α_{1B} are expressed in the ganglia? and (2) what is their relative abundance in the ganglia? Such information is critical to establish the composition of the α_{1B} transcripts expressed in the ganglia and ultimately to know which isoform(s) of α_{1B} underlies the N channel current expressed in sympathetic neurons. Figure 2A summarizes the results of the "nearest neighbor" RT-PCR analysis from the three reactions. All PCR-derived clones from the first group (i.e., 5′ end of the coding region) contained a guanosine at nt530 encoding G177; none encoded E177. A415 was encoded in ~50% of clones derived from the first and second groups. ~30% of clones from the second and third groups contained the 12 bases encoding SFMG (nt 3705–nt3716). Finally, the majority of clones from the third group (~80%) contained nt4674–nt4675 encoding ET. Furthermore, analysis of 12 of the very longest α_{1B} cDNA clones (4.7–5.4 kb; Figure 2B) isolated from the oligo dT–primed rat SCG cDNA library confirms the RT-PCR analysis. The majority, i.e., 11/12 of the longest clones, isolated from the cDNA library contained the six-base insert between

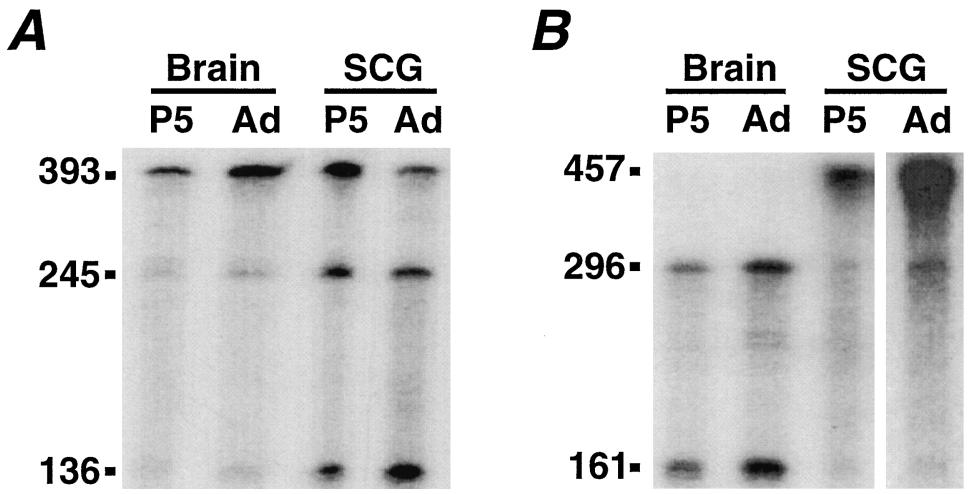

Figure 3. SFMG and ET Are Differentially Expressed in Sympathetic Ganglia and Brain

RNase protection analysis of RNA isolated from brain and SCG of adult (Ad) and 5-day-old (P5) rats.
(A and B) Gel separation of RNase digested ^{32}P-labeled SFMG (A) and ET (B) probes hybridized to RNA isolated from brain and ganglia. The undigested probes contain either SFMG (393 bases, A) or ET (457 bases, B), and the appearance of two additional bands following digestion indicates the presence of RNA lacking these sites. The predicted lengths of fully protected and partially digested probes are indicated. Average values for RNase protection analysis were: in ganglia: +SFMG, Ad = 39% ± 3%, n = 3; +SFMG, P5 = 41% ± 2%, n = 6; +ET, Ad = 87% ± 1%, n = 3; +ET, P5 = 82% ± 1%, n = 4; in brain: +SFMG, Ad = 76% ± 4%, n = 4; +SFMG, P5 = 75% ± 5%, n = 4; +ET, Ad = 5% ± 1%, n = 4; +ET, P5 = 9% ± 2%, n = 3. At least two different batches of RNA were used for each set of experiments. RNA products were separated on a 5% acrylamide gel, and relative band intensities were calculated using a phosphorimager.

nt4674–5 encoding ET. In the 5 clones that spanned nt3716 and contained the truncated form of the 3′UTR, we found that in every case, the region nt3705–nt3716 encoding SFMG was absent (Figure 2B). Figure 2C summarizes the overall results and indicates that at least six different variants of α_{1B} are potentially expressed in the ganglia but, based on our findings, two forms of α_{1B} that we refer to as rn$\alpha_{1B\text{-}a}$ and rn$\alpha_{1B\text{-}b}$ (see Table 2 in Experimental Procedures) and which differ only in the expression of A415, together account for 70%–80% of all transcripts.

Finally, we performed RNase protection assays using probes overlapping the three potential sites of RNA splicing to provide independent confirmation of the relative abundance of the different α_{1B} variants in sympathetic ganglia. The results were consistent with those obtained from the RT-PCR analysis (57% +A415; 41% ± 2% +SFMG, n = 9; 84% ± 4% +ET, n = 7; see Figure 3) and unambiguously confirm the expression of multiple splice variants of Ca^{2+} channel α_{1B} RNA in ganglia. RNA isolated from ganglia of P5 and adult rats was analyzed by RNase protection using probes overlapping the SFMG (Figure 3A) and ET (Figure 3B) sites. The presence of multiple variants of α_{1B} in the ganglia (SCG) is most clearly apparent in Figure 3A, where three bands corresponding to the fully protected labeled probe (393 bases; +SFMG) and two fragments digested at the SFMG site and corresponding to the partially protected probe (245 and 136; ΔSFMG) are visible.

SFMG and ET Sequences Are Differentially Expressed in Ganglia and Brain

Figures 3A and 3B show that the composition of brain α_{1B} RNA is different with respect to the expression of the SFMG and ET sites compared to ganglia. In brain, SFMG containing (75% ± 3%, n = 8; Figure 3A) and ET lacking (93% ± 3%, n = 7; Figure 3B) α_{1B} transcripts dominate and, as in ganglia, we found no consistent difference between the pattern of expression in P5 compared to adult tissue (see Figure 3). Our findings are consistent with the published sequence of rbB-I, the first rat brain–derived N channel clone, which also contains the SFMG sequence but lacks ET (Dubel et al., 1992; see Figure 7). Unlike SFMG and ET, the expression of A415 did not appear to be tissue specific. RNase protection analysis of brains of adult and P5 rats indicated 52% of α_{1B} RNA lacked A415 (data not shown).

Different Variants of α_{1B} Encode N Channels with Different Gating Kinetics

Having shown that different variants of α_{1B} are expressed in sympathetic ganglia and brain (Figures 2 and 3), we next tested the possibility that they encode functionally distinct isoforms of the N channel. SFMG and ET are located in the putative S3-S4 extracellular linkers in domains III and IV, respectively, of the α_{1B} subunit, in close proximity to the putative voltage–sensor regions, IIIS4 and IVS4. We therefore compared the functional properties of clones rn$\alpha_{1B\text{-}b}$ (+A415, ΔSFMG, +ET; ganglia dominant) and rn$\alpha_{1B\text{-}d}$ (+A415, +SFMG, ΔET; brain dominant) heterologously expressed with the rat brain Ca^{2+} channel β_3 subunit (rbβ_3, gift from K. Campbell and D. Witcher) in Xenopus oocytes to determine whether they encode functionally different N channels. Our findings, which are summarized in Figure 4 and Table 1, indicate significant differences between rn$\alpha_{1B\text{-}b}$ and rn$\alpha_{1B\text{-}d}$ in the macroscopic rates of channel activation ($p < 0.005$) and inactivation ($p < 0.05$) and in the voltage dependence of activation ($p < 0.0005$). Compared to rn$\alpha_{1B\text{-}b}$, rn$\alpha_{1B\text{-}d}$ currents activate and inactivate on average 1.7-fold and 4-fold

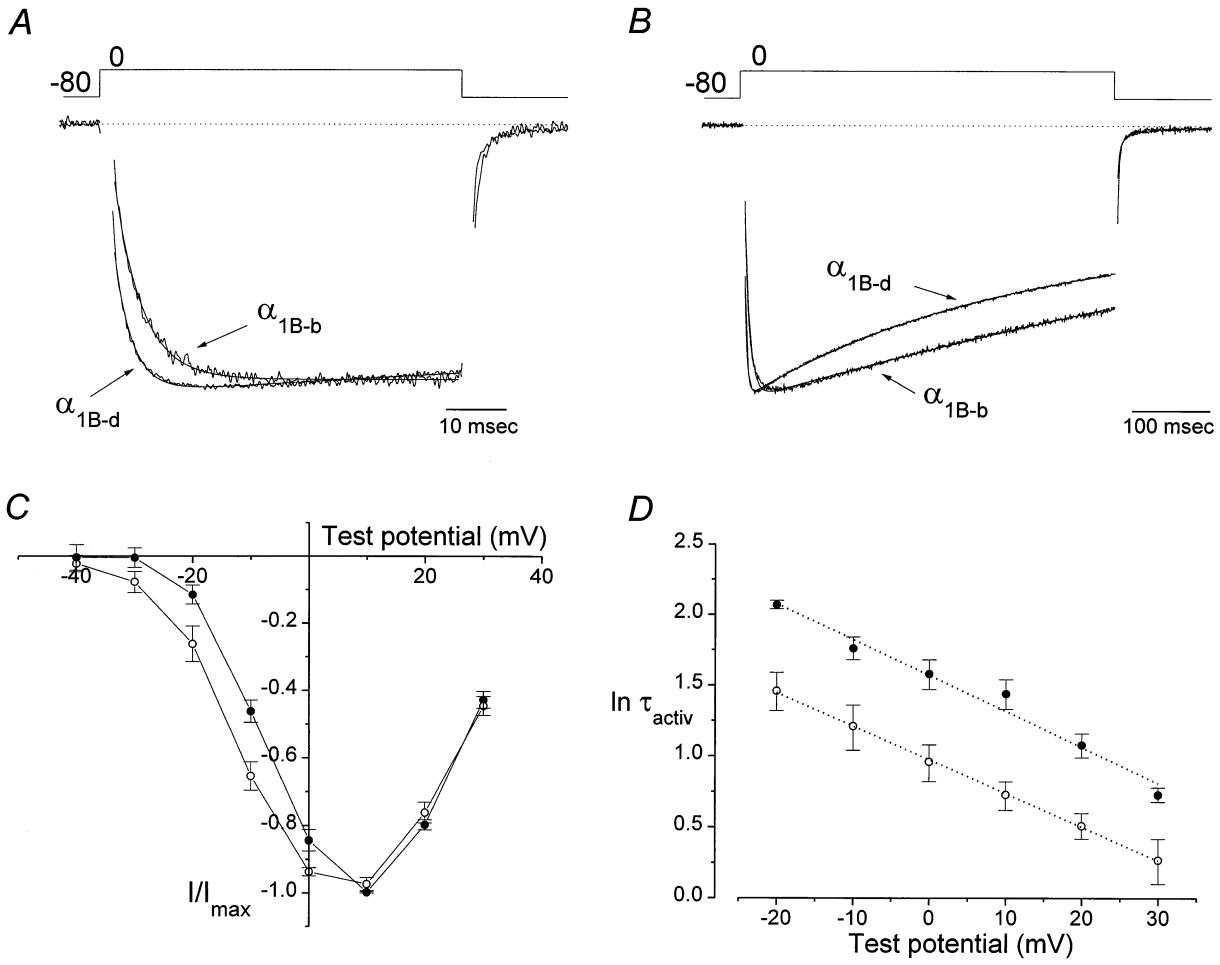

Figure 4. The Rates of Activation and Inactivation of Currents Induced by the Expression of rn$\alpha_{1B\text{-}b}$ and rn$\alpha_{1B\text{-}d}$ Are Different

(A) Different activation rates of rn$\alpha_{1B\text{-}b}$ and rn$\alpha_{1B\text{-}d}$ are apparent in the comparison of averaged normalized currents obtained from four oocytes expressing rn$\alpha_{1B\text{-}b}$ and five oocytes expressing rn$\alpha_{1B\text{-}d}$, together with the rat brain Ca^{2+} channel β_3 subunit, rbβ_3. Averaged, normalized currents are shown superimposed together with their respective best-fit exponentials curves, with activation time constants of τ_{act} = 4.6 ms for rn$\alpha_{1B\text{-}b}$ and τ_{act} = 3.0 ms for rn$\alpha_{1B\text{-}d}$. Recordings included in this analysis were limited to those in which the voltage clamp settled within ~2 ms.

(B) Different inactivation rates of rn$\alpha_{1B\text{-}b}$ and rn$\alpha_{1B\text{-}d}$ currents are apparent in the comparison of averaged, normalized currents obtained from six oocytes expressing rn$\alpha_{1B\text{-}b}$ and six oocytes expressing rn$\alpha_{1B\text{-}d}$. In these recordings, currents were induced by more prolonged depolarizations, and the sum of two exponentials (activation and inactivation) were fit to each averaged current. For rn$\alpha_{1B\text{-}b}$, τ_{inact} = 1472 ms, and for rn$\alpha_{1B\text{-}d}$, τ_{inact} = 333 ms.

(C) A small difference in the voltage-dependence of channel activation between the two clones is apparent in the comparison of the normalized, averaged peak current-voltage plots calculated from 11 oocytes expressing rn$\alpha_{1B\text{-}b}$ (closed circles; mean ± SEM) and 13 oocytes expressing rn$\alpha_{1B\text{-}d}$ (open circles; mean ± SEM).

(D) A semilogarithmic plot of the average activation time constants fit to currents obtained at different potentials from four oocytes expressing rn$\alpha_{1B\text{-}b}$ (closed circles) and five oocytes expressing rn$\alpha_{1B\text{-}d}$ (open circles; except at +30 mV, n = 4). Linear regression fits to the data are shown (dotted lines); for rn$\alpha_{1B\text{-}b}$, slope = −0.025 mV^{-1}, and y-intercept = 1.57; for rn$\alpha_{1B\text{-}d}$, slope = −0.024 mV^{-1}, and y-intercept = 0.98.

faster, respectively (Figures 4A and 4B), and activate at potentials 5 mV more negatively (Figure 4C).

Having established a significant difference in the voltage dependence of channel activation and the macroscopic rates of channel activation and inactivation between these two clones, we next determined whether a 5 mV difference in the activation threshold could account for the observed 1.7-fold difference in the macroscopic rate of channel activation between rn$\alpha_{1B\text{-}b}$ and rn$\alpha_{1B\text{-}d}$. Figure 4D demonstrates that activation rates for rn$\alpha_{1B\text{-}b}$ and rn$\alpha_{1B\text{-}d}$ are significantly different over a range of test potentials (−20 to +30 mV), but that both show the same dependency on voltage (e-fold change in τ_{act} for a 40 mV change in voltage). According to this relationship, the 5 mV shift in the voltage dependence of activation measured between clones rn$\alpha_{1B\text{-}b}$ and rn$\alpha_{1B\text{-}d}$ would result in a 1.13-fold difference in τ_{act}, a value that is insufficiently large to account for the observed differences in the macroscopic activation kinetics of these two clones (Table 1).

Robust Heterologous Expression of rnα_{1B} in Xenopus Oocytes in the Absence of a Ca^{2+} Channel β Subunit

Heterologous expression of α_{1B} alone, in Xenopus oocytes and HEK293 cells, reportedly occurs with very

Table 1. Properties of N Currents Recorded from Oocytes Expressing rnα_{1B-b} and rnα_{1B-d} in the Absence and Presence of rbβ_3

	Peak I (μA)	τ_{act} (msec)	τ_{inact} (msec)	$V_{1/2}$ act (mV)	$V_{1/2}$ inact (mV)
$\alpha_{1B-d} + \beta_3$	2.16 ± 0.60 (13)	3.4 ± 0.5 (5)	363 ± 33 (7)	−13.8 ± 0.9 (13)	−53 ± 3 (4)
$\alpha_{1B-b} + \beta_3$	2.11 ± 0.95 (10)	5.8 ± 0.5 (4)	1567 ± 558 (6)	−9.1 ± 0.7 (10)	−50 ± 3 (4)
α_{1B-d}	0.66 ± 0.12 (11)	3.3 ± 0.3 (4)	317 ± 30 (11)	−11.5 ± 0.4 (11)	−49 ± 2 (5)
α_{1B-b}	0.54 ± 0.10 (10)	N.D.	N.D.	−6.2 ± 0.3 (10)	−43 ± 1 (6)

Values shown are means ± SEM and the numbers of individual cells analyzed are indicated in brackets after each value. Estimates of peak current amplitudes (Peak I); activation (τ_{act}, at −10 mV) and inactivation (τ_{inact} at 0 mV) time constants; the midpoint of the rising phase of the current-voltage curve ($V_{1/2}$ act) and; the midpoint of the steady-state inactivation curve ($V_{1/2}$ inact). The activation and inactivation time constants for cells expressing α_{1B-b} alone could not be determined (N.D.) from these cells because of either the presence of tail currents or the slow time course of the voltage clamp. However, in a separate batch of recordings obtained under slightly different recording conditions, we have confirmed that the activation time constant of the N current induced by the expression of rnα_{1B-b} and rnα_{1B-d} in the absence of a heterologously expressed Ca^{2+} channel β subunit differ by 1.7-fold (α_{1B-b}: τ_{act} = 4.8 ± 0.3, n = 13; α_{1B-d}: τ_{act} = 2.8 ± 0.1, n = 13).

low efficiency, and in the majority of studies, cloned N channel currents have only been studied in cells heterologously expressing α_{1B} together with a Ca^{2+} channel β subunit (Stea et al., 1993, 1995; Williams et al., 1992; except see Roche et al., 1995). Coexpression of α_{1B} with a Ca^{2+} channel β subunit dramatically increases Ca^{2+} channel expression efficiency over that observed with α_{1B} alone (Williams et al., 1992), and the presence of the β subunit is considered essential to obtain "normal" N channel gating kinetics (Stea et al., 1993). Methods to improve the expression efficiency of α_{1B} in Xenopus oocytes include the use of nuclear injection of α_{1B} cDNA (Stea et al, 1993, 1995) and the construction of a chimeric clone in which the first 211 bases of α_{1B} are replaced with 513 bases of the 5′ end of $\alpha 1_A$ (Ellinor et al., 1994). In the present study, we utilized the pBSTA expression vector containing α_{1B} inserts flanked by the Xenopus β globin UTR sequences. The pBSTA vector has been shown to enhance the stability and translatability of foreign cRNA injected into Xenopus oocytes (Goldin and Sumikawa, 1992). Using the pBSTA expression vector, we observed robust expression of N channel currents with 5 mM Ba^{2+} as the charge carrier within 2–4 days following cytoplasmic injection of 13.8–23 ng of rnα_{1B} cRNA alone (0.61 ± 0.08 μA at +10 mV, n = 21 oocytes injected with 23 ng of rnα_{1B}; see also Figure 5). In contrast, N channel expression efficiency was significantly lower in oocytes injected with equivalent amounts of cRNA directly transcribed from rnα_{1B} in pBluescript (0.18 ± 0.06 μA at +10 mV, n = 9). The basic features of Ca^{2+} channel currents recorded from an oocyte expressing rnα_{1B-d} (+SFMG/ΔET; see Table 2 in Experimental Procedures) shows, somewhat unexpectedly, that coexpression of a Ca^{2+} channel β subunit is not necessary for the manifestation of currents with gating kinetics similar to those of the native N channel (Table 1). Specifically, Ca^{2+} channel currents induced by the expression of various rnα_{1B} clones alone do not display the slow activation gating kinetics typically reported in other studies (rbB-I; Stea et al., 1993). When BAPTA was used to prevent activation of the endogenous Cl_{Ca} current (which would otherwise obscure the true time course of N channel gating; Experimental Procedures and see Neely et al., 1993), the macroscopic activation, inactivation, and deactivation kinetics of Ca^{2+} channel currents induced by the expression of rnα_{1B-d} in the absence of a Ca^{2+} channel β subunit were "fast" (τ_{act} = 3–5 ms, τ_{inact} = 0.3–1.5 s; Table 1; Figures 5A and 6B) and within a factor of 2 of estimates from native N channel currents in rat sympathetic neurons (τ_{act} = 1–2 ms; Ikeda, 1991; τ_{inact} = 0.1–1.0 s; see Bean, 1989b; Plummer et al., 1989; Hess, 1990). Like the native N channel current, heterologously expressed rnα_{1B} currents inactivated as the holding potential was depolarized ($V_{1/2} \sim -50$ mV; Figure 5B and Table 1), and currents were irreversibly inhibited by low concentrations of ω-CgTx GVIA (200 nM; Figure 5C). We did not observe measurable Ca^{2+} channel currents in uninjected oocytes nor in those injected with rbβ_3 and rbα_2 in the absence of rnα_{1B} with 5 mM Ba^{2+} as the charge carrier.

Coexpression of the Ca^{2+} Channel rbβ_3 Subunit with rnα_{1B} Increases the Size of the Expressed Current without Increasing the Rate of Channel Activation

Consistent with previous reports (Williams et al., 1992; Stea et al., 1993), coexpression of the Ca^{2+} channel subunit (rbβ_3) significantly ($p < 0.025$) enhanced the peak amplitude of Ca^{2+} channel currents recorded in oocytes expressing α_{1B}. The peak Ca^{2+} channel current amplitude was 3.5-fold greater on average in oocytes coexpressing the rat brain–derived β_3 subunit (rbβ_3) with rnα_{1B} clones (2.14 ± 0.52 μA, n = 23 oocytes; Table 1; Figure 6A). Surprisingly, and in contrast to previous reports, the presence of rbβ_3 did not significantly speed the macroscopic activation or the inactivation gating kinetics of rnα_{1B} currents (τ_{act} = 3.3 ms and 3.4 ms at −10 mV; τ_{inact} = 317 ms and 363 ms at 0 mV; in the absence and presence of β_3, respectively; see Figures 6B and 6D and Table 1). There was, however, a small (2 mV) but significant ($p < 0.025$) negative shift in the voltage dependence of activation of Ca^{2+} channel currents recorded from oocytes coexpressing rnα_{1B-d} and rbβ_3 compared to those only expressing rnα_{1B-d} (Figure 6C).

Discussion

Multiple Variants of α_{1B} Are Expressed in Sympathetic Ganglia

We have demonstrated that multiple variants of the α_{1B} subunit, which encode N channels, are expressed in sympathetic ganglia. These variants are distinguished by the presence or absence of three discrete sequences in the coding region of the α_{1B} transcript (A415, SFMG, and ET) and a fourth in the 3′UTR. We also show that G177, which lies in a highly conserved S3 transmembrane region of the α_{1B} subunit, is invariant in RNA derived from sympathetic ganglia (see Figure 7). In rat brain

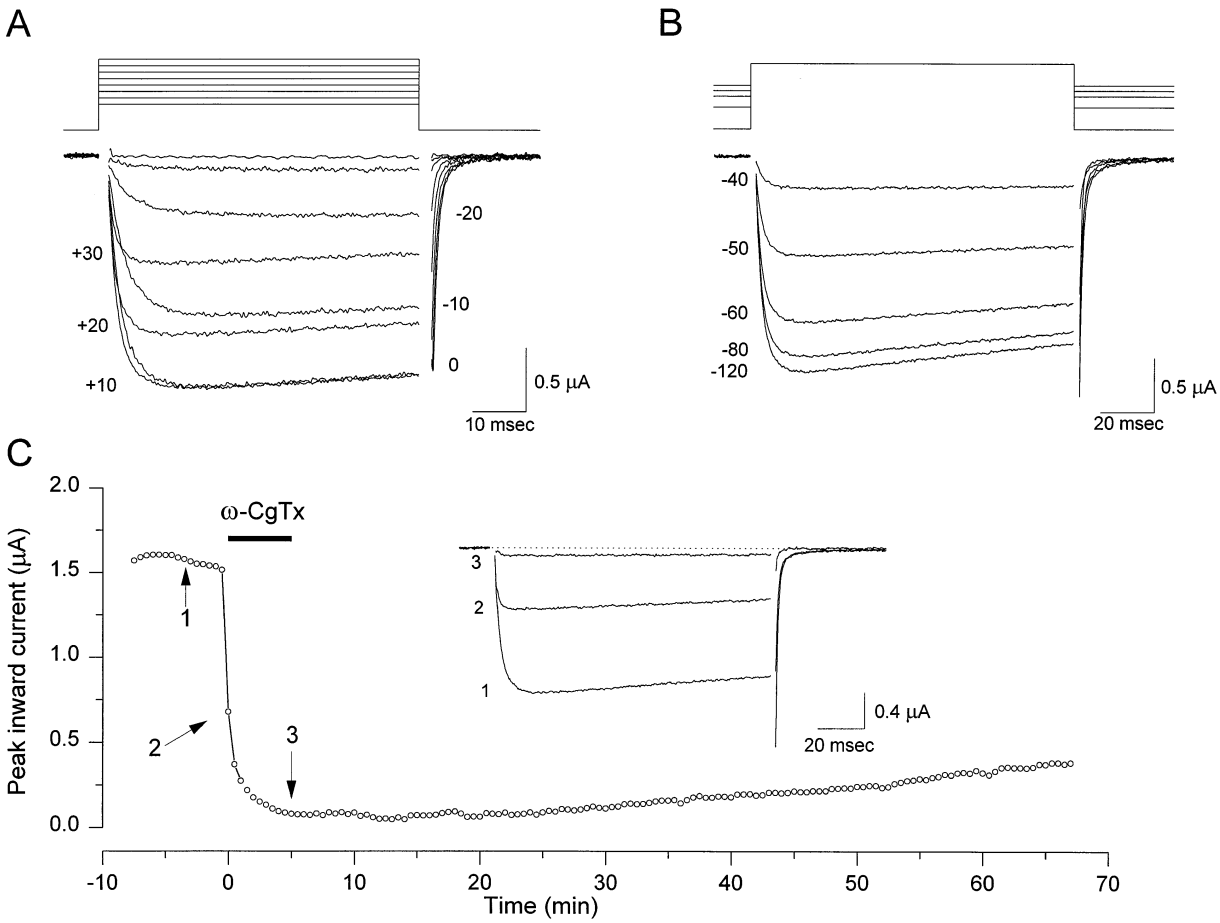

Figure 5. Robust Expression of N Currents in an Oocyte Heterologously Expressing only the α_{1B} Subunit

(A–C) Ca^{2+} currents recorded from an oocyte using 5 mM Ba^{2+} as the charge carrier injected 8 days earlier with 23 ng of Ca^{2+} channel rnα_{1B-d} cRNA.

(A) A series of N channel currents activated by depolarizations from a holding potential of −80 mV to different test potentials shows voltage dependence and activation kinetics similar to those of native N channels.

(B) A series of Ca^{2+} channel currents activated by depolarizations to a fixed test potential of 0 mV from different holding potentials (−120 to −40 mV) demonstrates steady-state inactivation characteristics.

(C) Rapid, irreversible inhibition of the N current by 200 nM ω-conotoxin GVIA. Peak current amplitudes are plotted, and currents were activated by test depolarizations to 0 mV applied once every 40 s from a holding potential of −80 mV. The solid bar indicates the time of exposure to ω-conotoxin GVIA, and sample traces at time points indicated by the arrows 1, 2, and 3 are shown as an inset.

in contrast, variants of α_{1B} expressing either E177 (rbB-I) or G177 (rbB-II) have been identified (Dubel et al., 1994, Soc. Neurosci., abstract). Our conclusions, that multiple variants of α_{1B} are expressed in the ganglia, are based on a combination of results from RT-PCR analysis, cDNA library screening, RNase protection assays, and DNA sequencing. We do not, however, exclude the presence of additional variant sites that could give rise to other forms of the α_{1B} transcript despite the fact that DNA sequencing of the entire length of the coding region of α_{1B} did not reveal any other variant sites apart from those described. α_{1B} clones differing in the expression of A415, which is located in the putative I-II intracellular linker of the α_{1B} subunit, and the tetrapeptide sequence SFMG in the putative extracellular linker between IIIS3-S4 have also been identified in mouse neuroblastoma cells (±A415; Coppola et al., 1994) and rat brain (±A415 and ±SFMG variants; Dubel et al., 1994, Soc. Neurosci., abstract). In addition, the expression of the dipeptide sequence ET, located in the putative extracellular linker between IVS3-S4 of the α_{1B}-subunit, varies with tissue type. Specifically, ET is present in α_{1B} clones derived from mouse (Coppola et al., 1994) and human (Williams

Table 2. Nomenclature Used in This Study for the Four rnα_{1B} Clones

Clone	A415	SFMG	ET
rnα_{1B-a}	−	−	+
rnα_{1B-b}	+	−	+
rnα_{1B-c}	−	+	−
rnα_{1B-d}	+	+	−

We use rn to refer to rat neuronal-derived clones and have adopted the naming scheme suggested by Birnbaumer et al. (1994) to identify each individual isoform (α_{1B-a} through α_{1B-d}). The isoforms are distinguished on the basis of the presence or absence of three discrete sequences encoding A415, SFMG, and ET as indicated. All rnα_{1B} clones encode G177 and, apart from the differences described, are identical in all other regions to the rat brain-derived clone, rbB-I (Dubel et al, 1992).

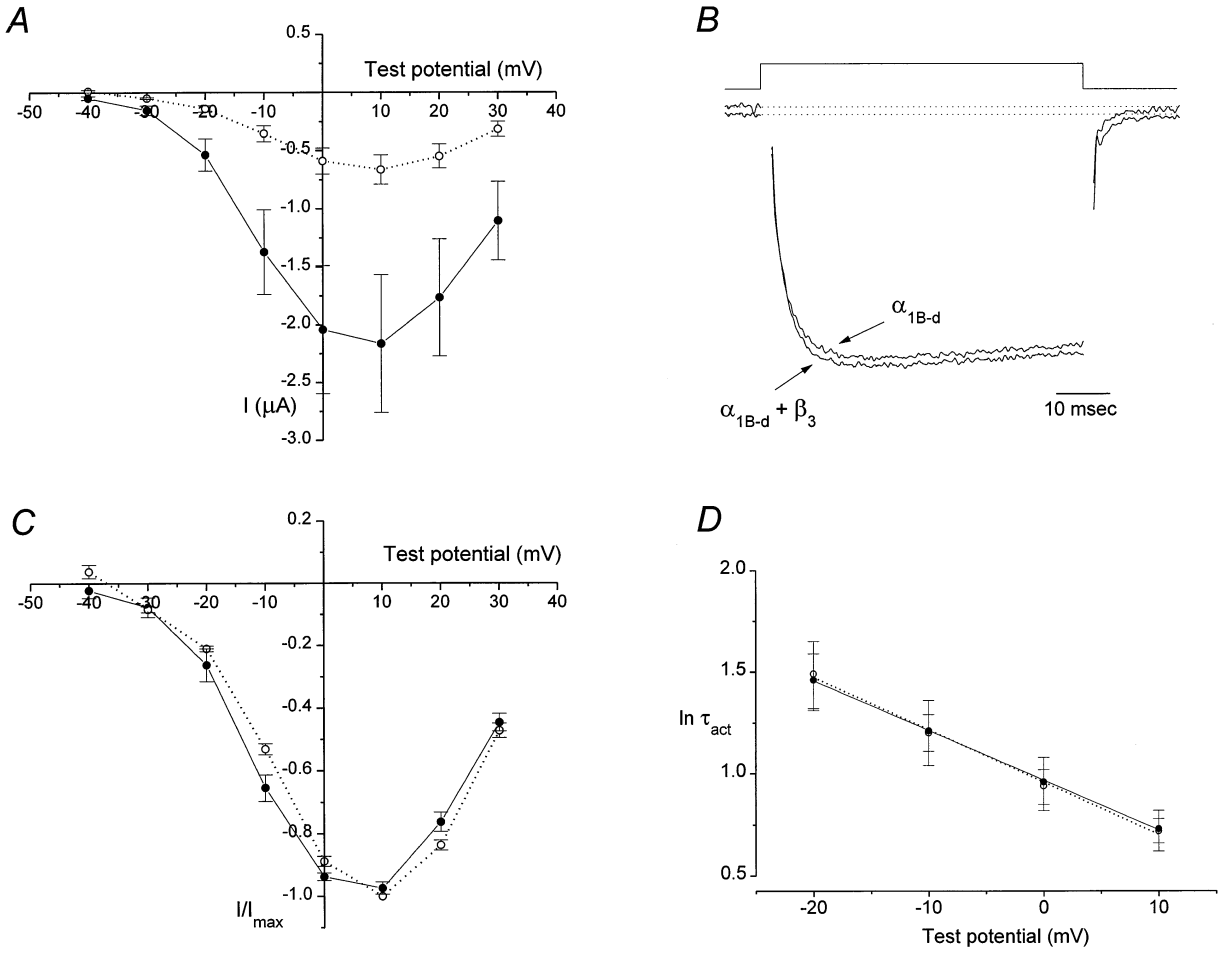

Figure 6. Coexpression of the Ca^{2+} Channel β_3 Subunit with rnα_{1B} Augments Ca^{2+} Channel Current Expression but Does Not Significantly Speed Channel Activation Kinetics

(A) The β_3 subunit significantly augments expression of N channel currents in Xenopus oocytes also expressing α_{1B}. Averaged peak current-voltage plots measured from oocytes expressing rn$\alpha_{1B\text{-}d}$ alone (open circles, dotted line; n = 13) and in the presence of β_3 (closed circles, solid line; n = 11). Points are means ± SEM.

(B) Superimposition of two individual currents from two different oocytes expressing rn$\alpha_{1B\text{-}d}$ alone and in the presence of the β_3 subunit. The displayed currents, are averaged and normalized to their respective peaks (1.1 μA and 1.6 μA for rn$\alpha_{1B\text{-}d}$ alone and for rn$\alpha_{1B\text{-}d}$ + β_3, respectively) and displayed offset with respect to each other in the vertical plane; the dotted lines indicate the respective zero current levels. Currents were activated by depolarizations to 0 mV from a holding potential of −80 mV.

(C) Normalized, averaged, peak current-voltage plots calculated from oocytes expressing rn$\alpha_{1B\text{-}d}$ (dotted line, open circles) and rn$\alpha_{1B\text{-}d}$ in the presence of β_3 (solid line, closed circles) for the same data and presented in A. The presence of the β_3 subunit induces a small negative shift (3 mV) in the voltage dependence of channel activation.

(D) Semilogarithmic plots of activation time constants, fit to currents induced by the expression of rn$\alpha_{1B\text{-}d}$ (n = 4; dotted line, open circles) and rn$\alpha_{1B\text{-}d}$ in the presence of β_3 (n = 5; solid line, closed circles) at different test potentials. The linear regression lines are drawn through the data and intercept the X-axis at Y = 0.96 and 0.97 and have slopes = −0.0257 mV_{-1} and −0.0244 mV^{-1}, for rn$\alpha_{1B\text{-}d}$ (dotted line) and rn$\alpha_{1B\text{-}d}$ + β_3 (solid line), respectively.

et al., 1992) neuroblastoma cells but thus far has not been reported in any brain-derived α_{1B} clone (rat: Dubel et al., 1992; rabbit: Fujita et al, 1993; see Figure 7). Our study is the first of its kind, however, to show that multiple variants of all three sites are expressed in a single tissue and as described below provides the first attempt to reconstruct the most abundantly expressed N channel isoforms in ganglia and brain.

The variant site within the 3′UTR generated α_{1B} transcripts with the most divergent sequence. Our analysis indicates that the majority of α_{1B} mRNAs contain a long 3′UTR (~2.6 kb) while in ~10% of transcripts, this region is truncated 194 bases into the 3′UTR. Recently, we have performed RNase protection assays that not only confirm the dominance of α_{1B} transcripts containing long 3′UTRs in the ganglia (75%–90%) but also demonstrate a similar pattern of expression of these variants in brain (S. H. and D. L., unpublished data). Interestingly, a similar truncation in the 3′UTR of α_{1B} clones derived from mouse neuroblastoma cells has been described; however, in these cells, it is the truncated form of α_{1B} that is most abundant (Coppola et al., 1994). The functional significance of the expression of two variants of the 3′UTR is not clear but could reflect important mechanisms for

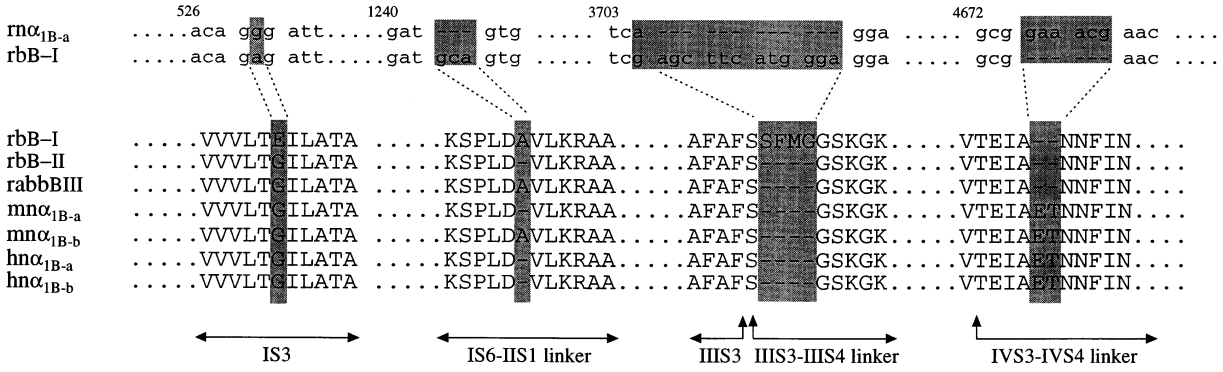

Figure 7. Sequence Comparisons between Different Mammalian Ca^{2+} Channel α_{1B} Subunits

Top, DNA sequences of clone rnα_{1B-a} and the rat brain-derived clone, rbB-I (Dubel et al., 1992), are compared in the four regions of divergence. Bottom, amino acid sequence comparisons at four divergent sites within α_{1B} for two rat brain–derived clones rbB-I (Dubel et al., 1992) and rbB-II (Dubel et al., 1994); a rabbit brain clone rabbBIII (Fujita et al., 1993); two mouse neuroblastoma clones mnα_{1B-a} and mnα_{1B-b} (Coppola et al., 1994), and two human neuroblastoma clones hnα_{1B-a} and hnα_{1B-b} (Williams et al., 1992).

regulating RNA localization or stabilization (Sachs, 1993). Inspection of the long form of the 3′UTR suggests that it contains at least 25 AU-rich destabilizing elements (Shaw and Kamen, 1986; Wilson and Treisman, 1988; Greenberg et al., 1990), several of which are clustered close to the poly(A) tail in a pattern similar to that found in the 3′UTR of the c-fos message (Greenberg et al., 1990). The short form of the α_{1B}-3′UTR in contrast contains none of these destabilizing elements. AU-rich regions in the 3′UTR of other genes are thought to increase lability of mRNA by promoting deadenylation of the poly(A) tail (Wilson and Treisman, 1988).

Composition of the Major Forms of α_{1B} Expressed in Sympathetic Ganglia and Brain

To determine the composition of α_{1B} transcripts expressed in the ganglia, and by extension the molecular identity of the α_{1B} subunit underlying the N channel current expressed in sympathetic neurons, we analyzed pairs of variant sites by RT-PCR analysis. Combining the RT-PCR analysis with results from RNase protection assays and library screening, we demonstrate that: (1) 60%–85% of α_{1B} mRNA in the ganglia is encoded by two splice variants (rnα_{1B-a} and rnα_{1B-b}; see Table 2), both of which lack SFMG but contain ET, and differ only in whether A415 is present or absent; (2) the remaining α_{1B} RNA in the ganglia is composed of up to four different variants and; (3) the expression of A415, SFMG, and ET are probably controlled by similar but independent mechanisms since in each case the processing of the site involves either a deletion or insertion of 3–12 bases, but the expression of no two variant sites appears to be linked.

Alternative splicing of RNA, which has been shown to generate variants of the α_{1C} class of Ca^{2+} channel in rat brain (Snutch et al., 1991), is the most likely mechanism by which the expression of variants of α_{1B} are regulated in ganglia and brain. Consistent with this, we have localized a 500 base intron in genomic DNA, which is located within the A415 codon (between nt1243 and nt1244). A consensus sequence for RNA splicing lies within this intron, which, together with the presence of two alternate 3′ splice acceptor sites, almost certainly determines the expression of ±A415 variants (S. H., Z. L., and D. L.; unpublished data). The expression of the SFMG and ET sites, in contrast to A415, is tissue specific. Using RNase protection assays, we show that α_{1B} RNA isolated from the brains of adult and P5 rats gives a pattern of expression of SFMG and ET (75%–90%, +SFMG/ΔET) that is the converse of that seen in sympathetic ganglia (60%–85%, ΔSFMG/+ET). It will therefore be extremely interesting to determine the mechanisms and molecules responsible for regulating the tissue specific expression of these two sites, particularly because they encode functionally different channels. It is noteworthy that SFMG and ET are located in equivalent sites of the two homologous domains, III and IV, of the α_{1B} subunit, which are believed to have evolved from a common ancestral gene (see Hille, 1992b).

Functional Significance of the Expression of Variants of α_{1B}

A415, located in the putative IS6-IIS1 cytoplasmic linker of the α_{1B} subunit, as far as we can tell appears to have little influence on the gating of the N channel. In contrast, the sequences SFMG and ET in the S3-S4 extracellular linkers of domains III and IV, respectively, appear to be localized to a region that is critical in regulating channel gating. This finding has important implications on several fronts:

(1) Together with our RNase protection assays, we predict that the dominant N channel isoform expressed in sympathetic ganglia (60%–85%, ΔSFMG/+ET) activates and inactivates more slowly and at voltages 5 mV more positive than the isoform that dominates in the brain (75%–90%, +SFMG/ΔET). It is highly likely therefore that differential expression of N channels with slightly different activation thresholds and gating kinetics influence the rate, duration, and voltage dependence of transmitter release at these functionally different synapses. In sympathetic ganglia the N channel has been shown to dominate in regulating Ca^{2+}-dependent release of catecholamines (Hirning et al., 1988). A more

slowly inactivating N channel might therefore be optimal for supporting a more sustained release of catecholamines from presynaptic sympathetic varicosities, where the transmitter must diffuse relatively long distances to reach the postsynaptic target cell. In brain, in contrast, the preferential expression of a more rapidly gating form of the N channel might be optimal for mediating fast synaptic transmission. N channels are preferentially localized to synaptic regions in the brain (Westenbroek et al., 1992; Elliot et al., 1995) and have been shown to participate primarily with the P-type channels in mediating release of neurotransmitters both excitatory and inhibitory synapses (Luebke et al., 1993; Takahashi and Momiyama, 1993; Wheeler et al., 1994; see also Dunlap et al., 1995). Although most whole-cell N channel currents recorded from a variety of CNS neurons exhibit both rapidly and slowly inactivating components (rat hippocampal pyramidal cells: Fisher et al., 1990; Mogul and Fox, 1991; mouse motor neurons: Mynlieff and Beam, 1992; and neuroblastoma–glioma cell line: Kasai and Neher, 1992), N-like currents recorded in isolated nerve terminals of the rat neurohypophysis are exclusively of the rapidly inactivating form (Lemos and Nowycky, 1989), which is consistent with our findings. Many other factors, however, can and will influence N channel gating kinetics, thus emphasizing the importance of using criteria other than inactivation kinetics to distinguish different components of the macroscopic N channel current in native cells (see also Bean, 1989b; Aosaki and Kasai, 1989; Jones and Marks, 1989; Kongsamut et al., 1989; Plummer et al., 1989, for similar discussions of criteria used to distinguish N from L channel currents). For example, variability in N channel gating kinetics may stem from interaction of the channel with other proteins, including tonically activated G proteins (Kasai, 1991), syntaxin (Bezprozvanny et al., 1995), or different auxiliary subunits (Scott et al., 1996).

(2) Our study provides the first indication that transcripts encoding functionally distinct isoforms of the N channel are coexpressed in rat sympathetic ganglia. At least 60% of α_{1B} transcripts encode N channel currents with relatively slower rates of channel activation (τ = 5–6 ms) and inactivation ($\tau \sim 1.5$ s), but up to 40% of the α_{1B} variants activate (τ = 3–4 ms) and inactivate (τ = 300–400 ms) with a relatively faster time course. This raises the possibility that multiple, functionally distinct isoforms of α_{1B} might be expressed in individual cells, which would be expected to generate two kinetically distinct N currents distinguished most readily at the macroscopic level by their different inactivation time courses ($\tau_{fast} \sim 300$ ms, $\tau_{slow} \sim 1.5$ s). Consistent with this hypothesis, several groups have reported the presence of kinetically distinct N channel currents with different rates of inactivation in whole-cell recordings and single channel recordings from both rat (Aosaki and Kasai, 1989; Plummer et al., 1989; Plummer and Hess, 1991) and frog (Jones and Marks, 1989; Kongsamut et al., 1989) sympathetic neurons. To date, the only explanation offered for the presence, in individual cells, of distinct N channel currents with different rates of inactivation has centered on the proposed interconversion between different conformational states distinguished by their different rates of inactivation (Plummer and Hess, 1991). The similarity between estimates of the inactivation time courses of the two native N channel currents in sympathetic neurons (τ_{fast} = 100–200 ms and τ_{slow} > 400 ms; Jones and Marks, 1989; Kongsamut et al., 1989; Plummer et al., 1989) and those of the isoforms rn$\alpha_{1B\text{-}b}$ and rn$\alpha_{1B\text{-}d}$ ($\tau_{fast} \sim 300$ ms, $\tau_{slow} \sim 1.5$ s) is consistent with our hypothesis that molecularly distinct α_{1B} subunits, at least in part, underlie the different N currents seen in the native cell.

(3) SFMG and ET are located in the two extracellular linkers between S3 and S4 of domains III and IV, respectively, and close to the putative voltage sensor (S4). Our findings that alterations in the S3-S4 linker significantly affect channel gating kinetics are consistent with mutational analysis of L-type Ca^{2+} channels (Nakai et al., 1994) and of *Shaker* K channels (Mathur et al., 1996, Biophysics, abstract). In their studies, Nakai et al. (1994) and Mathur et al. (1996, Biophysics, abstract) demonstrate that the S3-S4 linkers of domain I of the L-type Ca^{2+} channel α_1 subunit and of the *Shaker* K channel subunit, respectively, are critical determinants for the kinetics of voltage-dependent channel activation. In our studies, the N channel inactivates with a fairly rapid time course (compared for example to the L channel), and the macroscopic time constants of activation and inactivation are significantly different between the S3-S4 variants. We cannot therefore ascribe the observed differences in the gating kinetics between the two S3-S4 variants exclusively to differences in either channel activation or inactivation mechanisms since, at the macroscopic level, these two processes are not readily separable. Nonetheless, our analyses of rn$\alpha_{1B\text{-}b}$-induced and rn$\alpha_{1B\text{-}d}$-induced currents rule out a simple mechanism involving a change in the voltage dependence of channel activation since the measured 5 mV shift between the two variants is simply not sufficient to account for the observed 1.7-fold difference in the macroscopic rate of channel activation. Yang and Horn (1996) recently demonstrated that the IVS4 helix of the voltage-gated Na^+ channel translocates through the hydrophobic core of the protein during channel activation. It is possible, therefore, that the length (Mathur et al., 1996, Biophysics, abstract) or secondary structure (Nakai et al., 1994) of the S3-S4 linker in voltage-gated ion channels might physically restrain the adjoining S4 helix and alter its rate of movement through the membrane. Additional experiments will be needed to determine the relative contributions of the two S3-S4 linkers in domains III (SFMG) and IV (ET) of the α_{1B} subunit; however, it is clear that the S3-S4 extracellular linker is emerging as a critical domain whose composition may finely tune the gating kinetics of several voltage-gated ion channel families (Nakai et al., 1994; Mathur et al., 1996, Biophysics, abstract).

A Ca^{2+} Channel β Subunit Is Not Required for Expression of N Channel with Normal Gating Kinetics

A surprising observation that stems from our functional analysis of the ganglia-derived α_{1B} clones is that expression of N channel currents in Xenopus oocytes, with characteristics very similar to those of the native channel, does not require the heterologous expression of a

Ca^{2+} channel β subunit. In addition, coexpression with $rb\beta_3$, which induced a 3.5-fold increase in the overall Ca^{2+} channel current density compared to α_{1B} alone, did not significantly affect the macroscopic rate of N channel activation. In these respects, our findings are at odds with the consensus view in the field, which supports a critical role of the Ca^{2+} channel β subunit in achieving efficient expression of the N channel (Williams et al., 1992; Stea et al., 1993) and for the acquisition of normal channel phenotype (see also Lacerda et al., 1991; Stea et al., 1993), presumably by directly binding to the α_1 subunit (Pragnell et al., 1994). The single most striking difference between our studies and those of others is the high level of expression of N channel currents achieved in oocytes following the expression of α_{1B} alone. Our use of the Xenopus β globin expression vector (pBSTA; Goldin and Sumikawa, 1992) resulted in >15-fold improved expression efficiency of $rn\alpha_{1B}$ clones (0.6 μA with 5 mM Ba^{2+}) compared to similar expression studies in Xenopus oocytes using the rat brain clone rbB-I (0.04 μA with 40 mM Ba^{2+}; Stea et al., 1993). Currents induced by the heterologous expression of α_{1B} alone activated (τ_{act} = 3–5 ms) and inactivated (τ_{inact} = 0.3–1.5 s) with rates comparable to those of the native N current in rat sympathetic neurons (τ_{act} = 1–2 ms and τ_{inact} = 0.1–>1.0 s; see Bean, 1989a; Plummer et al., 1989; Hess, 1990; Ikeda, 1991) and much faster than rates reported previously (τ_{act} = 60–70 ms for rbB-I; Stea et al., 1993). The N channel clone used in our studies differs from rbB-I by only a single base at nt530, which converts the E177 in rbB-I to a G177 in $rn\alpha_{1B\text{-}d}$. While it is possible that a difference of one strategically placed amino acid could account for the observed 12- to 20-fold difference in the activation kinetics of rbB-I and $rn\alpha_{1B\text{-}d}$, the 15-fold difference in overall expression efficiency must also be considered as a potentially important factor. Indeed, a recent study of L channel currents heterologously expressed in myotubes has demonstrated a striking correlation between L channel gating kinetics and the level of expression (Adams et al., 1996). Specifically, Adams et al. (1996) report activation time constants of L channel gating ranging from ~20 ms, in cells expressing a high density of channels, to ~100 ms in cells with a low channel density. Although no definitive explanation has been offered to account for these findings, the possibility that proteins endogenous to the myotube, such as G proteins or ancillary subunits, could affect channel gating is discussed (Adams et al., 1996). It is noteworthy that N channel currents heterologously expressed in Xenopus oocytes can be modulated by tonically active endogenous G proteins (Roche et al., 1995) and that a slowing in the activation kinetics of N channel gating is one of the main affects of G protein–mediated inhibition (Wanke et al., 1987; Bean, 1989a; see Hille, 1992a). If a limited number of activated G proteins are available in the oocyte, then the degree of G protein–mediated inhibition and consequently the extent to which the activation kinetics are slowed would be directly correlated with the level of expression of the α_{1B} subunit. This scenario, which implies that the underlying activation kinetics of the N channel current might be masked in cells expressing low levels of protein could also explain the lack of an effect of the Ca^{2+} channel β subunit in cells in which the level of protein expression is already high. Alternatively, it is possible that injection of Ca^{2+} channel cRNA into oocytes stimulates the expression of an endogenous β subunit, which associates with and modulates the activity of the heterologously expressed N channel. There is evidence that injection of large amounts of several different cRNAs encoding a variety of membrane proteins can induce the expression of a hyperpolarization-activated current in Xenopus oocytes (Tzounopoulos et al., 1995). In our case, the expression of a Xenopus β subunit would have to account for the rapid gating kinetics of N channels induced by the expression of α_{1B} alone and for the lack of effect of heterologously expressed $rb\beta_3$ of N channel gating kinetics, even though a molar excess of $rb\beta_3$ was injected along with $rn\alpha_{1B}$ in these experiments.

Summary

We have identified and characterized the α_{1B} clones most likely underlying the N channel in rat sympathetic neurons and shown that robust heterologous expression of α_{1B} can be achieved in the absence of a Ca^{2+} channel β subunit. We hypothesize that the expression of functionally distinct isoforms of α_{1B} might underlie the presence of kinetically distinct N currents observed in recordings from native cells. In addition, our finding that kinetically distinct isoforms of the N channel are differentially expressed in the peripheral and central nervous system suggests an important mechanism for finely tuning the efficacy of synaptic transmission at morphologically and functionally distinct synapses.

Experimental Procedures

RT-PCR and "Nearest Neighbor" Analysis of Variant Sites within α_{1B} Transcripts

mRNA was isolated from superior cervical ganglia of 4- to 5-day-old rats essentially as described by Lin et al. (1996). The majority of RNA isolated from the ganglia originates from sympathetic neurons, which is by far the most abundant cell in this tissue, and contributions of RNA derived from nonneuronal cells of superior cervical ganglia of newborn rats has been shown to be <10% (Mandelzys et al., 1994). First strand cDNA was synthesized from ~375 ng of mRNA using SuperScript RNase H- Reverse Transcriptase (Gibco BRL) either randomly primed or primed with 1 μM of the α_{1B}-specific primer Bd4479 (ACTCATAAGGGGCATCGTAGAAC). The resulting cDNA was used as template in the "nearest neighbor" PCR analysis of variant sites within the pool of α_{1B} cDNAs. This method was designed to obtain information on the association between the four potential sites of sequence variation in α_{1B}, G177/E177, ±A415, ±SFMG, and ±ET, and in addition to provide an estimate of their relative abundance of expression in the ganglia. The large size of the full-length coding region (>7 kb) made other approaches less tractable. The following three primer pairs were used to amplify "nearest neighbor" variant sites: For G177/E177 → ±A415: Bu376 (ATGTCTGAACGACTGGATGACAC) and Bd1318 (GACCCAGCAGC ACAGAGGTCTAC); for ±SFMG → ±ET: Bu3483 (CAGCATTGCCCT GGCTGCTGAGG) and Bd4813 (GATGAAGAACAGCATGGCAATG AG); and for ±A415 → ±SFMG: Bu1084 (GAGCGGGAGCGAGTCGA GAACCG) and Bd3853 (AGACATTCTTCAGAGAGTTCACC). We were able to obtain longer PCR products containing more than two potential variant sites, but the subcloning efficiency of these longer PCR-derived products was too low for detailed analysis. Similar PCR-based approaches have been used to estimate the relative abundance of RNA splice variants of the glutamate receptor in brain (Ruano et al., 1995). The PCR was performed using the Expand High

Fidelity kit (Boehringer Mannheim) in a 50 μl reaction mix containing 5 μl of the cDNA (93.75 ng mRNA), 2.6 U enzyme mix, 1 × PCR buffer, 1.5 mM $MgCl_2$, 200 μM of each deoxynucleotide, and 0.3 μM of each primer. The amplification was performed with the following program using a Perkin Elmer 9600: 2 min at 95°C × 1; 10 s at 94°C, 30 s at 62°C, 2 min at 68°C × 10; 10 s at 94°C, 30 s at 62°C, 2 min + 20 s at 68°C × 20; and 7 min at 68°C × 1. The PCR-derived cDNAs from each reaction were then subcloned in pGEM T vector (Promega), and their identity was confirmed by a combination of DNA sequencing (for the G177/E177 site) and restriction digest analysis (for the ±A415, ±SFMG, and ±ET sites).

RNase Protection Assays

Total RNA was purified from whole brain and ganglia of adult and 5-day-old rats using a guanidium thiocyanate and phenol–chloroform extraction protocol (adapted from Chomczynski and Sacchi, 1987). ^{32}P-labeled antisense RNA probes overlapping A415 (nt1084–1340), SFMG (nt3460–3853), and ET (nt4379–4836) were constructed from linearized plasmids (pGEM-T vector) containing appropriate PCR-derived subclones using the Maxi-script kit (Ambion). Probes were gel purified and stored as ethanol precipitates. Hybridization and digestion conditions were essentially the same as those described in DeKonick and Cooper (1995). Ten micrograms of total RNA from brain or 3 μg of total RNA from SCG and 2 × 10^5 cpm of probe were coprecipitated and resuspended in 30 μl hybridization buffer containing 60% formamide, 0.4 M NaCl, 10 mM EDTA, and 40 mM PIPES (pH 6.4). Samples were denatured at 85°C and allowed to hybridize overnight at 60°C. After hybridization, the samples were digested in a 350 μl reaction mix containing: 0.3 M NaCl, 5mM EDTA, 3.5 μl of the RNase Cocktail (Ambion), and 10 mM Tris (pH 7.5). Samples were then treated with proteinase K, extracted, and precipitated with 10 μg of tRNA as carrier. After resuspension in 30 μl formaldehyde loading buffer, the samples were denatured and separated on a 5% polyacrylamide gel. The gel was exposed first to a phosphor imaging plate to quantitate relative band intensities (Fuji JAS 1000) and subsequently exposed to film with an intensifying screen for 2–4 days at −80°C.

Rat Superior Cervical Ganglia cDNA Library Construction and Screening

Two custom cDNA libraries were constructed (Stratagene) from mRNA isolated from superior cervical ganglia of 4- to 5-day-old rats (Sprague Dawley) and used to screen for α_{1B} cDNAs. A bidirectional cDNA library (Lambda Zap II, EcoRI; Stratagene) containing inserts of >1 kb was oligo dT and random primed and enriched in 5′ Ca^{2+} channel α_1 subunit sequences by the inclusion of a degenerate primer, (5′- [T/C]TC[T/C]CC[A/T/G][G/C][T/A][G/A/T/C]/AC-3′) predicted to be located ~1 kb downstream of the 5′ end of the α_1 transcripts. A second unidirectional cDNA library (Lambda Uni-ZAP, EcoRI-XhoI; Stratagene), oligo dT primed and enriched in 3′ sequence, was size fractionated into two pools containing inserts of 0.4–4 kb and >4 kb, respectively. Phage rscg95101 was isolated from the 5′-enriched cDNA library after screening 4.5 × 10^5 plaque forming units of an amplified titre with a randomly primed 621bp HindIII fragment of rbB-I (nt1–621; Dubel et al., 1992) and after 2 × plaque purification was transformed into pBluescript. The long insert 3′-enriched cDNA library (>4 kb pool) was highly enriched in Ca^{2+} channel α_1 sequences; a screen of 5 × 10^5 plaque forming units of an unamplified titre with a randomly primed, ~8.7 kb NotI-SpeI fragment of rbB-I (nt25–8768) yielded 67 positives, 57 of which were confirmed by PCR to contain α_{1B} sequence. Five phage isolates, rscg9404, rsg9407, rscg9408, rscg9411, and rscg9414, were transformed into pBluescript after three rounds of plaque purification. pBS clones rscg95101 and rscg9408 were subjected to double strand sequencing using Sequenase V2.0 (United States Biochemical). pBS clones rscg9404, rscg9407, rscg9411, rscg9414 were subjected to analysis by restriction digest, PCR, and partial DNA sequencing.

Construction of Full-Length rnα_{1B} cDNAs

rn$\alpha_{1B\text{-}a}$ (G, ΔA415, ΔSFMG, +ET) was constructed by ligating a 2.2 kb SpeI (in pBluescript)-Psp1406 I (nt2106) fragment of clone rsg95101 and a 6.6 kb RsrII (nt 3510)–SpeI (in pBluescript) fragment of clone rscg9408 with a 1.4 kb Psp1406 I (nt2106)-RsrII (nt3510) fragment of a PCR-derived clone rscg95102. The 7.3 kb cDNA insert was then transformed into pBluescript II SK (−) to yield clone rn$\alpha_{1B\text{-}a}$. For expression in Xenopus oocytes, a 7.3 kb SpeI-KpnI digested fragment of rn$\alpha_{1B\text{-}a}$ was cloned into the pBSTA vector. The pBSTA expression vector contains the 5′ and 3′ untranslated regions of the Xenopus β globin gene and has been shown to enhance the stability and translatability of certain messages, thereby increasing protein expression (Goldin and Sumikawa, 1992). pBSTA rn$\alpha_{1B\text{-}a}$ was then used as the template for constructing three other isoforms, rn$\alpha_{1B\text{-}b}$, rn$\alpha_{1B\text{-}c}$, and rn$\alpha_{1B\text{-}d}$ (see Table 2). pBSTA rn$\alpha_{1B\text{-}b}$ was constructed by replacing a ~1.4 kb PmlI-PmlI fragment of rn$\alpha_{1B\text{-}a}$ (nt986–2413) with the equivalent site digested from rbB-I (Dubel et al., 1992). pBSTA rn$\alpha_{1B\text{-}c}$ was constructed by replacing a ~3.5 kb SunI-Bg2 fragment of rn$\alpha_{1B\text{-}a}$ (nt2901–5470) with the equivalent site digested from rbB-I. Finally, pBSTA rn$\alpha_{1B\text{-}d}$ was constructed by replacing a ~1.4 kb PmlI-PmlI fragment of rn$\alpha_{1B\text{-}c}$ (nt987–2413) with the equivalent site digested from rbB-I.

Heterologous Expression in Xenopus Oocytes

In Vitro Transcription of cRNAs from α_{1B}, β_3, and α_2 cDNA

In vitro transcription was performed using the Ambion mMESSAGE mMACHINE Kit. Capped RNAs were synthesized with T7 or T3 RNA polymerase. Briefly, cRNAs were transcribed in a 20 μl reaction mix containing 2 μl 10× Transcription Buffer, 10 μl 2× Ribonucleotide Mix (15 mM ATP, CTP, UTP, 3 mM GTP, and 12 mM Cap GTP Analog), 1–2 μg linearized template cDNA, and 10× Enzyme Mix. The mixture was then incubated at 37°C for 2 hr, and the reaction was terminated by $LiCl_2$ precipitation (7.5 M $LiCl_2$ and 75 mM EDTA). After washing, the cRNA precipitate was resuspended in DEPC-treated H_2O and analyzed by gel electrophoresis or stored at −20°C. For transcription from rnα_{1B} clones, we routinely add 30 mM GTP to the reaction mix to improve yields of long cRNAs.

Oocyte Harvesting and Injection

Oocytes were surgically removed from Xenopus laevis frogs and prepared for injection by a 1–2 hr dissociation in collagenase (1.5 mg/ml) hours, followed by thorough rinsing in Ca^{2+}-free, enzyme-free OR2 solution and a 6–20 hr recovery period in ND-92 containing 10 mg/ml gentamycin. Defolliculated stage V–VI oocytes were carefully selected for injection. Of a 100–500 ng/μl cRNA solution, 46 nl was injected into each oocyte using a precision nanoinjector (Drummond). Oocytes were then stored at 19°C in ND92 solution for up to 2 weeks. Ca^{2+} channel currents were recorded within 2–3 days following injection of 300–500 ng/μl of rnα_{1B} alone or 100–300 ng/μl of rnα_{1B} coinjected with rbβ_3 cRNA. Ca^{2+} channel currents >5 μA (5 mM Ba^{2+}) have been recorded from oocytes for as long as 12 days after injection. Coexpression of rbβ_3 with α_{1B} was performed with a 1.5 M excess of rbβ_3 over α_{1B}. The Ca^{2+}-free OR2 solution contained 82.5 mM NaCl, 2 mM KCl, 1 mM $MgCl_2$, and 5 mM HEPES (pH adjusted to 7.4 with NaOH). The ND92 solution contained 92 mM NaCl, 2 mM KCl, 5 mM HEPES, 2 mM $MgCl_2$, 1.2 mM $CaCl_2$, and 50 μg/ml gentamycin (pH adjusted to 7.4 with NaOH).

Recording from Oocytes

Macroscopic Ca^{2+} channel currents were recorded from oocytes using the two microelectrode recording technique with the use of the Warner oocyte voltage-clamp amplifier (OC-725b). A virtual ground circuit eliminated the need for series resistance compensation when recording large currents, and the use of a 3M KCl agar bridge, placed close to the oocyte and directly connecting the recording chamber to a AgCl pellet, minimized junction potentials associated with solution changes. Micropipettes of 1–2 MΩ when filled with 3M KCl were used for the voltage electrode and for the current electrode; the tip of the electrode was broken down to obtain resistances of 0.3–0.5 MΩ. Oocytes expressing Ca^{2+} channel currents had resting membrane potentials of ~−40 to −50 mV when impaled with two electrodes. A grounded metal shield was placed between the two electrodes to increase the settling time of the clamp. In ideal recordings, the current following a voltage step settled within ~2 ms.

Recording Solutions and Inhibiting the Activation of the Endogenous Ca^{2+}-Activated Cl^- Current

Oocytes were injected with 46 nl of a 50 mM solution of BAPTA (1,2-bis(o-aminophenoxy)ethane-N,N,N',N'-tetraacetate) at least 15 min prior to recording (Neely et al., 1993; Charnet et al., 1994; Roche

et al., 1995). We have found this to be an essential step to prevent activation of the endogenous Ca^{2+}-activated Cl^- current (Cl_{Ca}), which is apparently also activated by Ba^{2+} (Vernino et al., 1994). Niflumic acid was not effective and even in oocytes injected with BAPTA, Cl_{ca} was still activated in some cells when the Ba^{2+} current exceeded 4–5 μA. Activation of Cl_{ca} depended on the influx of Ba^{2+} and appeared as a slowly activating ($\tau > 100$ ms) and a slowly deactivating ($\tau > 10$–50 ms) inward current at depolarized potentials (in low external Cl^-; see below). Due to the slow activation kinetics of this current, its presence particularly distorted the inactivation kinetics of the underlying Ca^{2+} channel current. All recordings exhibiting slowly deactivating tail currents were excluded from the analyses of channel gating kinetics. N channel currents were recorded using 5 mM $BaCl_2$, 85 mM tetraethylammonium, 5 mM KCl, and 5 mM HEPES (pH adjusted to 7.4 with methanesulphonic acid) (the presence of 5 mM Cl^- was essential for the 3 M KCl bridge).

Data Acquisition and Analysis of Macroscopic Currents

Data were acquired on line and leak subtracted using a P/4 protocol (PClamp V6.0; Axon Inst). Voltage steps were applied usually every 10–20 s from a holding potential of −80 mV. Ca^{2+} channel currents recorded under these conditions showed little run-down over the duration of the recordings, which could last >1 hr. Activation kinetics were only analyzed in those recordings in which the voltage clamp settled within ~2 ms and only from recordings digitized at 10 kHz. Estimates of the inactivation time constants were obtained only from currents activated by 480 ms depolarizations, which still was not sufficiently long to provide an accurate estimate of the slow time constants characteristic of rm$\alpha_{1B\text{-}b}$ currents (>1.5 s). Both single exponential and the sum of two exponentials were fit to the data using curve-fitting routines in PClamp (Axon) and Origin (Microcal) to obtain best estimates of the activation and inactivation rates.

Acknowledgments

We thank Kevin P. Campbell and D. Witcher for rbβ_3; Terry P. Snutch for rbB-I and rbα_2 and Steve Dubel for providing us with sequence of the 3′UTR of rbB-I; and Ellis Cooper and laboratory for helping set up the RPA. We are grateful to Justin Fallon, Edward Hawrot, and Pascal Bochet for reading and commenting on the manuscript and to Steve Jones for insightful discussions. Yingxin Lin assisted in some experiments. Supported in part by National Institutes of Health Predoctoral Training Grant GM07601 and was done in partial fulfillment of the requirements for a Ph.D. degree from Brown University (to Z. L.). Supported by NS29967 and a gift from Miles Pharmaceuticals to D. L.

Received September 16, 1996; revised November 1, 1996.

References

Adams, BA, Tanabe, T, and Beam, KG. (1996). Ca current activation rate correlates with α_1 subunit density. Biophys. J. *71*, 156–162.

Aosaki, T., and Kasai, H. (1989). Characterization of two kinds of high-voltage-activated Ca-channel currents in chick sensory neurons. Differential sensitivity to dihydropyridines and omega-conotoxin GVIA. Pflugers Arch. *414*, 150–156.

Bean, B.P. (1989a). Neurotransmitter inhibition of neuronal calcium currents by changes in channel voltage dependence. Nature *340*, 153–156.

Bean, B.P. (1989b). Classes of calcium channels in vertebrate cells. Annu. Rev. Physiol. *51*, 367–384.

Bezprozvanny, I., Scheller, R.H., and Tsien, R.W. (1995). Functional impact of syntaxin on gating of N-type and Q-type calcium channels. Nature *378*, 623–626.

Birnbaumer, L,. Campbell, K.P., Catterall, W.A., Harpold, M.M., Hofmann, F., Horne, W.A., Mori, Y., Schwartz, A., Snutch, T.P., Tanabe, T., and Tsien, RW. (1994). Matters arising: the naming of voltage-gated calcium channels. Neuron *13*, 505–506.

Charnet, P., Bourinet, E., Dubel, S.J., Snutch, T.P., and Nargeot, J. (1994). Calcium currents recorded from a neuronal α_{1C} L-type calcium channel in Xenopus oocytes. FEBS Lett. *344*, 87–90.

Chomczynski, P., and Sacchi, N. (1987). Single-step method of RNA isolation by acid guanidinium thiocyanate-phenol-chloroform extraction. Ann. Biochem. *162*, 156–159.

Coppola, T., Waldmann, R., Borsotto, M., Heurteaux, C., Romey, G., Mattei, M.-G., and Lazdunski, M. (1994). Molecular cloning of a murine N-type calcium channel α_1 subunit. Evidence for isoforms, brain distribution, and chromosomal localization. FEBS Lett. *338*, 1–5.

Cox, D.H., and Dunlap, K. (1994). Inactivation of N-type calcium current in chick sensory neurons: calcium and voltage dependence. J. Gen. Physiol. *104*, 311–336.

Delcour, A.H., Lipscombe, D., and Tsien, R.W. (1993). Multiple modes of N-type Ca channel activity distinguished by differences in gating kinetics. J. Neurosci. *13*, 181–194.

De Koninck, P., and Cooper, E. (1995). Differential regulation of neuronal nicotinic ACh receptor subunit genes in cultured neonatal rat sympathetic neurons: specific induction of alpha 7 by membrane depolarization through a Ca2+/calmodulin-dependent kinase pathway. J. Neurosci. *15*, 7966–7978.

Dolphin, A.C. (1996). Facilitation of Ca^{2+} current in excitable cells. Trends Neurosci. *19*, 35–43.

Dubel, S.J., Starr, T.V., Hell, J.W., Ahlijanian, M.K., Enyeart, J.J., Catterall, W.A., and Snutch, T.P. (1992). Molecular cloning of the α_1 subunit of an ω-conotoxin-sensitive calcium channel. Proc. Natl. Acad. Sci. USA *89*, 5058–5062.

Dunlap, K., Luebke, J.I., and Turner, T.J. (1995). Exocytotic Ca^{2+} channels in mammalian central neurons. Trends Neurosci. *18*, 89–98.

Elmslie, K.S., Zhou, W., and Jones, S.W. (1990). LHRH and GTP-gamma-S modify calcium current activation in bullfrog sympathetic neurons. Neuron *5*, 75–80.

Elliott, E.M., Malouf, A.T., and Catterall, W.A. (1995). Role of calcium channel subtypes in calcium transients in hippocampal CA3 neurons. J. Neurosci. *15*, 6433–6444.

Ellinor, P.T., Zhang, J.-F., Horne, W.A., and Tsien, R.W. (1994). Structural determinants of the blockade of N-type calcium channels by a peptide neurotoxin. Nature *372*, 272–275.

Fisher, R.E., Gray, R., and Johnston, D. (1990). Properties and distribution of single voltage-gated calcium channels in adult hippocampal neurons. J. Neurophysiol. *64*, 91–104.

Fujita, Y., Mynlieff, M., Dirksen, R.T., Kim, M.-S., Niidome, T., Nakai, J., Friedrich, T., Iwabe, N., Miyata, T., Furuichi, T., Furutama, D., Mikoshiba, K., Mori, Y., Beam, KG. (1993). Primary structure and functional expression of the ω-conotoxin-sensitive N-type channel from rabbit brain. Neuron *10*, 585–598.

Goldin, A.L., and Sumikawa, K. (1992). Preparation of RNA for injection into Xenopus oocytes. Methods Enzymol. *207*, 279–297.

Greenberg, M.E., Shyu, A.B., and Belasco, J.G. (1990). Deadenylylation: a mechanism controlling c-fos mRNA decay. Enzyme *44*, 181–192.

Hess, P. (1990). Calcium channels in vertebrate cells. Annu. Rev. Neurosci. *13*, 337–356.

Hille, B. (1992a) G protein–coupled mechanisms and nervous signaling. Neuron *9*, 187–195.

Hille, B., ed. (1992b). Ionic Channels of Excitable Membranes. (Sunderland, Massachusetts: Sinauer Press).

Hille, B. (1994). Modulation of ion-channel function by G-protein-coupled receptors. Trends Neurosci. *17*, 531–535.

Hirning, L.D., Fox, A.P., McCleskey, E.W., Miller, R.J., Olivera, B.M., Thayer, S.A., and Tsien, R.W. (1988). Dominant role of N-type Ca^{2+} channels in evoked release of norepinephrine from sympathetic neurons. Science *239*, 57–61.

Ikeda, S.R. (1991). Double-pulse calcium channel current facilitation in adult rat sympathetic neurones. J. Physiol. *439*, 181–214.

Jones, S.W., and Marks, T.N. (1989). Calcium currents in bullfrog sympathetic neurons: II Inactivation. J. Gen. Physiol. *94*, 169–182.

Kasai, H. (1991). Tonic inhibition and rebound facilitation of a neuronal calcium channel by a GTP-binding protein. Proc. Natl. Acad. Sci. USA *88*, 8855–8859.

Kasai, H., and Neher, E. (1992). Dihydropyridine-sensitive and omega-conotoxin-sensitive calcium channels in a mammalian neuroblastoma-glioma cell line. J. Physiol. *448*, 161–188.

Kongsamut, S., Lipscombe, D., and Tsien, R.W. (1989). The N-type Ca channel in frog sympathetic neurons and its role in α-adrenergic modulation of transmitter release. Ann. N.Y. Acad. Sci. *560*, 312–333.

Lacerda, A.E., Kim, H.S., Ruth, P., Perez-Reyes, E., Flockerzi, V., Hofmann, F., Birnbaumer, L., and Brown, A.M. (1991). Normalization of current kinetics by interaction between the α_1 and β subunits of the skeletal muscle dihydropyridine-sensitive Ca^{2+} channel. Nature *352*, 527–530.

Lemos, J.R., and Nowycky, M.C. (1989). Two types of calcium channels coexist in peptide-releasing vertebrate nerve terminals. Neuron *2*, 1419–1426.

Lin, Z., Harris, C.A., and Lipscombe, D. (1996). The molecular identity of Ca channel α_1 subunits expressed in rat sympathetic neurons. J. Mol. Neurosci. *7*, 23–33.

Lipscombe, D., Kongsamut, S., and Tsien, R.W. (1989). α-adrenergic inhibition of sympathetic neurotransmitter release mediated by selective modulation of N-type calcium channel gating. Nature *340*, 639–642.

Luebke, J.I., Dunlap, K., and Turner, T.J. (1993). Multiple calcium channel types control glutamatergic synaptic transmission in the hippocampus. Neuron *11*, 895–902.

Mandelzys, A., Pie, B., Deneris, E.S., and Cooper, E. (1994). The developmental increase in ACh current densities on rat sympathetic neurons correlates with changes in nicotinic ACh receptor alpha-subunit gene expression and occurs independent of innervation. J. Neurosci. *14,* 2357–2364.

Mogul, D.J., and Fox, A.P. (1991). Evidence for multiple types of Ca2+ channels in acutely isolated hippocampal CA3 neurones of the guinea-pig. J. Physiol. (Lond.) *433*, 259–281.

Mynlieff, M., and Beam, K.G. (1992). Characterization of voltage-dependent calcium currents in mouse motoneurons. J. Neurophysiol. *68*, 85–92.

Nakai, J., Adams, B.A., Imoto, K., and Beam, K.G. (1994). Critical roles of the S3 segment and S3-S4 linker of repeat I in activation of L-type calcium channels. Proc. Natl. Acad. Sci. USA *91*, 1014–1018.

Neely, A., Wei, X., Olcese, R., Birnbaumer, L., and Stefani, E. (1993). Potentiation of the β subunit of the ratio of the ionic current to the charge movement in the cardiac calcium channel. Science *262*, 575–578.

Plummer, M.R., and Hess, P. (1991). Reversible uncoupling of inactivation in N-type calcium channels. Nature *351*, 657–659.

Plummer, M.R., Logothetis, D.E., and Hess, P. (1989). Elementary properties and pharmacological sensitivities of calcium channels in mammalian peripheral neurons. Neuron *2*, 1453–1463.

Pragnell, M., De Waard, M., Mori, Y., Tanabe, T., Snutch, T.P., and Campbell, K.P. (1994). Calcium channel β-subunit binds to a conserved motif in the I-II cytoplasmic linker of the α_1-subunit. Nature *368*, 67–70.

Rittenhouse, A.R., and Hess, P. (1994). Microscopic heterogeneity in unitary N-type calcium currents in rat sympathetic neurons. J. Physiol. *474*, 87–99.

Roche, J.P., Anantharam, V., and Treistman, S.N. (1995). Abolition of G protein inhibition of α_{1A} and α_{1B} calcium channels by co-expression of the β_3 subunit. FEBS Lett. *371*, 43–46.

Ruano, D., Lambolez, B., Rossier, J., Paternain, A.V., and Lerma, J. (1995). Kainate receptor subunits expressed in single cultured hippocampal neurons: molecular and functional variants by RNA editing. Neuron *14*, 1009–1017.

Sachs, A.B. (1993). Messenger RNA degradation in eukaryotes. Cell *74*, 413–421.

Shaw, G., and Kamen, R.A. (1986). A conserved AU sequence from the 3′ untranslated region of GM-CSF mRNA mediates selective mRNA degradation. Cell *46*, 659–667.

Scott, V.E., DeWaard, M., Hongyan, L., Gurnett, C.A., Venzke, D.P., Lennon, V.A., and Campbell, K.P. (1996). β subunit heterogeneity in N-type Ca channels. J. Biol. Chem. *271*, 3207–3212.

Snutch, T.P., Tomlinson, W.J., Leonard, J.P., and Gilbert, M.M. (1991). Distinct calcium channels are generated by alternative splicing and are differentially expressed in the mammalian CNS. Neuron *7*, 45–57.

Soong, T.W., Stea, A., Hodson, C.D., Dubel, S.J., Vincent, S.R., and Snutch, T.P. (1993). Structure and functional expression of a member of the low voltage-activated calcium channel family. Science *260*, 1133–1136.

Stea, A., Dubel, S.J., Pragnell, M., Leonard, J.P., Campbell, K.P., and Snutch, T.P. (1993). A β-subunit normalizes the electrophysiological properties of a cloned N-type Ca^{2+} channel α_1-subunit. Neuropharmacology *32* 1103–1116.

Stea, A., Soong, T.W., Snutch, T.P. (1995). Determinants of PKC-dependent modulation of a family of neuronal calcium channels. Neuron *15*, 929–940.

Takahashi, T., and Momiyama, A. (1993). Different types of calcium channels mediate central synaptic transmission. Nature *366*, 156–158.

Tzounopoulos, T., Maylie, J., and Adelman, J.P. (1995). Induction of endogenous channels by high levels of heterologous membrane proteins in Xenopus oocytes. Biophys. J. *69*, 904–908.

Vernino, S., Amador, M., Luetje, C.W., Patrick, J., and Dani, J.A. (1992). Calcium modulation and high calcium permeability of neuronal nicotinic acetylcholine receptors. Neuron *8*, 127–134.

Wanke, E., Ferroni, A., Malgaroli, A., Ambrosini, A., Pozzan, T., and Meldolesi, J. (1987). Activation of a muscarinic receptor selectively inhibits a rapidly inactivated Ca2+ current in rat sympathetic neurons. Proc. Natl. Acad. Sci. USA *84*, 4313–4317.

Westenbroek, R.E., Hell, J.W., Warner, C., Dubel, S.J., Snutch, T.P., and Catterall, W.A. (1992). Biochemical properties and subcellular distribution of an N-type calcium channel alpha-1 subunit. Neuron *9*, 1099–1115.

Wheeler, D.B., Randall, A., and Tsien, R.W. (1994). Roles of N-type and Q-type Ca2+ channels in supporting hippocampal synaptic transmission. Science *264*, 107–111.

Williams, M.E., Brust, P.F., Feldman, D.H., Patthi, S., Simerson, S., Maroufi, A., McCue, A.F., Velicelebi, G., Ellis, S.B., and Harpold, M.M. (1992). Structure and functional expression of an ω-Conotoxin-sensitive human N-type calcium channel. Science *257*, 389–395.

Wilson, T., and Treisman, R. (1988). Removal of poly(A) and consequent degradation of c-fos mRNA facilitated by 3′ AU-rich sequences. Nature *336*, 396–399.

Yang, N., George, A.L., and Horn, R. (1996). Molecular basis of charge movement in voltage-gated sodium channels. Neuron *16* 113–122.